Electronic Supplementary Material (ESI) for ChemComm.

Supporting Information

Vapour-phase deposition of oriented copper dicarboxylate metal-organic framework thin films

Timothée Stassin[a], Sabina Rodríguez-Hermida[a], Benedikt Schrode[b], Alex John Cruz[a,c], Francesco Carraro[d], Dmitry Kravchenko[a], Vincent Creemers[a], Ivo Stassen[a], Tom Hauffman[c], Dirk De Vos[a], Paolo Falcaro[d], Roland Resel[b] and Rob Ameloot*[a]

[a] Centre for Membrane Separations, Adsorption, Catalysis and Spectroscopy for Sustainable Solutions (cMACS), KU Leuven, Celestijnenlaan 200F box 2454, 3000 Leuven, Belgium.

[b] Institute of Solid State Physics, Graz University of Technology, Petersgasse 16, 8010 Graz, Austria.

[c] Department of Materials and Chemistry, Research group Electrochemical and Surface Engineering, Vrije Universiteit Brussel, Pleinlaan 2, 1050 Brussels, Belgium.

[d] Institute of Physical and Theoretical Chemistry, Graz University of Technology, Stremayrgasse 9/Z2, 8010 Graz, Austria.

*Correspondence to:

Prof. Rob Ameloot
Tel.: +32-1637-6674
Email: rob.ameloot@kuleuven.be

Contents

S1. Material and Methods 3
S2. CuO precursor characterisation 5
S3. Optical images of CuCDC, CuBDC and CP-CuBDC films 8
S4. CuCDC films from PVD CuO, PVD Cu and thermal CuO, on silicon and glass substrates 9
S5. CuBDC and CP-CuBDC films from PVD CuO, PVD Cu and thermal CuO, on silicon substrates 10
S6. AFM investigation of CuCDC, CuBDC and CP-CuBDC films 11
S7. CuCDC, CuBDC and CP-CuBDC film thickness from ellipsometry data 12
S8. Cross-sectional SEM images 13
S9. H_2BDC and H_2CDC linker thermogravimetric analysis 14
S10. ATR-FTIR analysis 15
S11. CuBDC oriented films: liquid-phase epitaxy vs CVD 17
S12. References 18

S1. Material and Methods

Substrates

Silicon and glass substrates were used for Cu and CuO PVD. The Si wafers were purchased with the following specifications: p-type, single-side polished back-etched, 76.2 mm diameter (Si-Mat Silicon Materials, Germany). These are <100> Si wafers with a resistivity of 1-30 ohm cm^{-1} and a thickness of 381 ± 25 µm. The glass substrates consisted of Pyrex 7740 glass disks with a diameter of 76.2 mm.

Cu and CuO precursor film deposition

Cu and CuO thin films were deposited through physical vapor deposition (PVD) with a BAE370 magnetron RF sputter coater, using Cu target (99.999% purity, Demaco) or a CuO target (99.9% purity, Demaco). The depositions took place at a pressure of ~7 10^{-3} mbar, under Ar plasma, at a set power of 150 W. The film thickness was varied through the deposition time. Thermal CuO was obtained by heating PVD Cu films at 300 °C in air for 15 min.

Solid-vapour reaction

CuCDC and (CP-)CuBDC films were obtained through solid-vapour reaction between Cu or CuO precursor and dicarboxylic acid vapours as follows. The Cu- or CuO-coated substrates were placed in a 300 mL Schlenk tube together with a glass boat containing 500 mg ligand. For reactions under dry conditions the tube was closed and evacuated (~10^{-1} mbar). For reaction under humidified conditions the tube was closed and evacuated (~10^{-1} mbar), and 100 µL water was subsequently inserted in the tube through a side port. The tube was then placed for 16 hours in a forced convection oven preheated at 200 °C. Afterwards the tube was removed from the oven and vented. The samples were removed from the tube while hot and left in the oven for 30 additional minutes for activation.

X-ray diffraction

GIXRD measurements were performed at the beamline ID10 at the European Synchrotron Radiation Facility (ESRF, Grenoble, France), using a wavelength of 1.54 Å, an incident angle of 0.19°, and a Pilatus 300K detector mounted on a goniometer arm approximately 335 mm from the sample. To investigate a larger volume of reciprocal space, the detector was set to several distinct goniometer positions and the obtained data were stitched during evaluation. Data were transformed to reciprocal space for analysis. All data conversion, treatment and analysis steps were performed with GIDVis.[1]

Scanning electron microscopy

Top-view SEM images were recorded using a Philips XL30 FEG. The samples were cleaved and then sputter coated with 5 nm of Pt prior to the inspection. Tilted-view and cross-sectional view SEM images were recorded with a Hitachi SU8000 microscope (SE detector) operating at an accelerating voltage of 10 kV. The samples were sputter coated with 1 nm Pt (Cressington 108) and then cleaved prior to the inspection.

X-ray reflectivity

X-ray reflectometry data was recorded on a Malvern PANalytical Empyrean diffractometer equipped with a PIXcel3D solid state detector using a Cu anode (Cu Kα1: 1.5406 Å; Cu Kα2: 1.5444 Å). Samples were placed on a programmable XYZ-stage. Before each measurement, an iterative alignment scheme was employed to optimize both sample height (z) and tilt (ω). Data were collected at room temperature in reflection geometry within a -0.03° - 4.5° 2θ range using a step size of 0.005 °.

Ellipsometry

Film optical properties were measured using an M-2000x spectroscopic ellipsometer (J. A. Woollam Co. Inc., λ = 246-1000 nm) at a fixed 65° incidence angle. The film thickness and optical constants were modelled and fitted using the CompleteEASE software in the range 400-1000 nm (J. A. Woollam Co. Inc.).

Atomic force microscopy

Samples were scanned using a PicoSPM (5500, Agilent Technologies) under ambient conditions, in tapping mode using Si cantilevers (AC160TS-R3). Data processing and analysis were carried out with WSXM 5.0.[2]

Infrared spectroscopy

Attenuated total reflection Fourier-transform infrared spectroscopy (ATR-FTIR) spectra were recorded on a Varian 670 FTIR spectrometer equipped with a VeeMAX^{TM} III accessory (PikeTech). The spectra were collected with a 60° Ge ATR crystal at an incidence angle of 60°. A ZnSe polarizer grid was mounted to obtain p-polarized light. 64 scans were accumulated by either a DLaTGS or MCT detector with a resolution of 4 cm^{-1}.

Thermogravimetric analysis

Thermogravimetric analysis was carried out under nitrogen atmosphere using a Netzsch STA 449 F3 Jupiter thermogravimetric analyser.

X-ray photoelectron spectroscopy

X-ray photoelectron spectroscopy (XPS) measurements were performed with a hemi-spherical PHI5600 Photoelectron Spectrometer (Physical Electronics). The spectrometer is equipped with an Al Kα monochromatic X-ray source of 1486.71 eV. Measurements were operated at a pressure of 4 x 10^{-9} Torr at an angle of incidence of 45°. Scans were taken at a pass energy of 23.5 eV with a 0.1 eV step size, and using a spot diameter of 0.8 mm.

Quartz crystal microbalance (QCM) porosimetry

Adsorption measurements were performed in a QCM environmental cell at room temperature. Controlled amounts of methanol were evaporated using a CEM evaporator (Bronkhorst®) in a set nitrogen carrier gas flow to obtain methanol vapour of desired concentration. The methanol vapour concentration was varied step-wise in the range 0-95%. At the end of each 120 s step the average frequency change measured during the last 30 s was calculated and plotted against the corresponding relative humidity value. The measurement was repeated between 7 and 12 times for statistics and noise reduction. 95% confidence intervals were calculated and plotted as well. The CuBDC and CuCDC films were grown from 15 nm PVD CuO deposited on the gold electrode of the QCM crystals, and activated for 16 h at 150 °C.

S2. CuO precursor characterisation

PVD CuO

Thickness

Table S1. Excellent agreement between PVD CuO film thickness measured by ellipsometry and XRR.

Method	PVD CuO thickness (nm)
Ellipsometry	10.7
XRR	10.3

Ellipsometry model and fit

Table S2. PVD CuO substrate ellipsometry model. The mean squared error (MSE) of the fit was 2.9.

Layer	Thickness (nm)
PVD CuO	10.7 nm
Native oxide (SiO_2)	1.74 nm
Silicon	Substrate

Optical constants

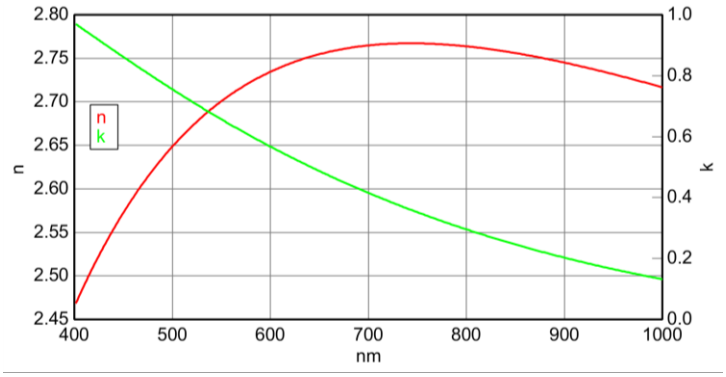

Figure S1. PVD CuO optical constants.

XRR

Table S3. PVD CuO substrate XRR model.

Layer	Thickness	Density (g cm^{-3})
PVD CuO	10.3	6.53
Native oxide (SiO_2)	1.94	1.94
Silicon	Substrate	2.33

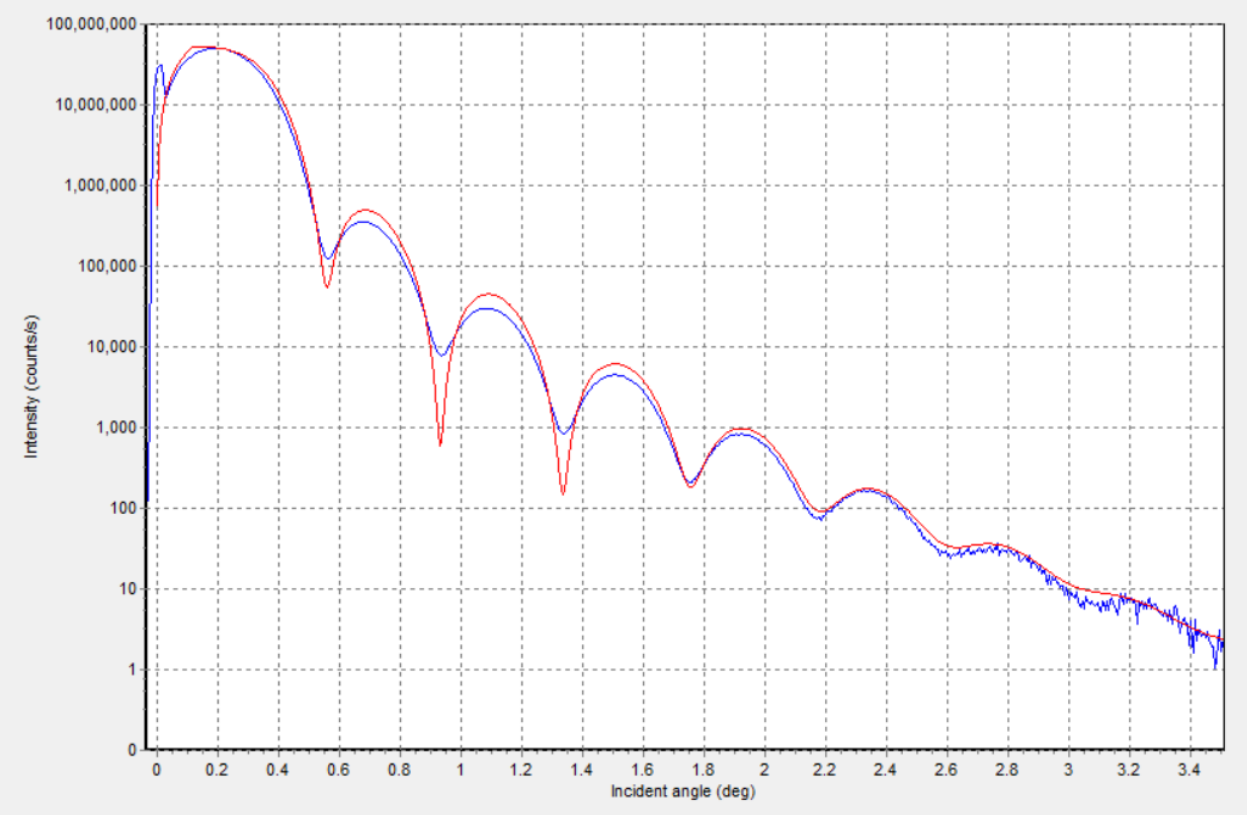

Figure S2. PVD CuO XRR data (blue) and fitted model (red).

Thermal CuO

Ellipsometry

Table S4. Thermal oxidation of PVD Cu to thermal CuO. Thickness from ellipsometry data.

PVD Cu thickness	nominal	10 nm
Thermal CuO thickness[a]	experimental	18 nm
Expansion factor	theoretical[b]	1.7
	experimental	1.8

[a]average of 5 measurements on 5 different spots on the surface.

[b]based on crystallographic densities.

XPS

XPS measurements on the precursor copper oxide deposited on Si-wafer are performed to check the oxidation state and stoichiometry. Obtained XPS spectra and peak fit data are shown in Figure S3 and Table S5, respectively. Apart from copper- and oxygen-related peaks, the survey scan reveals the presence of carbon surface contamination. Most importantly, Cu^{2+}-related satellites are visible in the Cu2p high-resolution scan, being characteristic for CuO whereas Cu_2O would not show these features.[3,4] The O1s signal shows two peaks, of which the lower binding energy peak (529.63 eV) is attributed to oxygen bound in CuO and the peak at higher binding energy (531.26 eV) to carbonates, hydroxyls or other surface

contamination.[3] For confirmation, the atomic ratio of Cu:O, considering only the low-binding energy O1s peak and summation over all Cu2p-related peaks (including satellites), is determined to

$$\frac{\mathrm{Cu}}{\mathrm{O}} = \frac{(\sum Cu2p)/(RSF_{\mathrm{Cu2p3}} + RSF_{\mathrm{Cu2p1}})}{O1s(\mathrm{CuO})/RSF_{\mathrm{O1s}}} = \frac{3238}{3224} = 1.00$$

Therefore, we conclude that Cu is fully oxidized to CuO, without any Cu_2O or metallic Cu present in the observation volume.

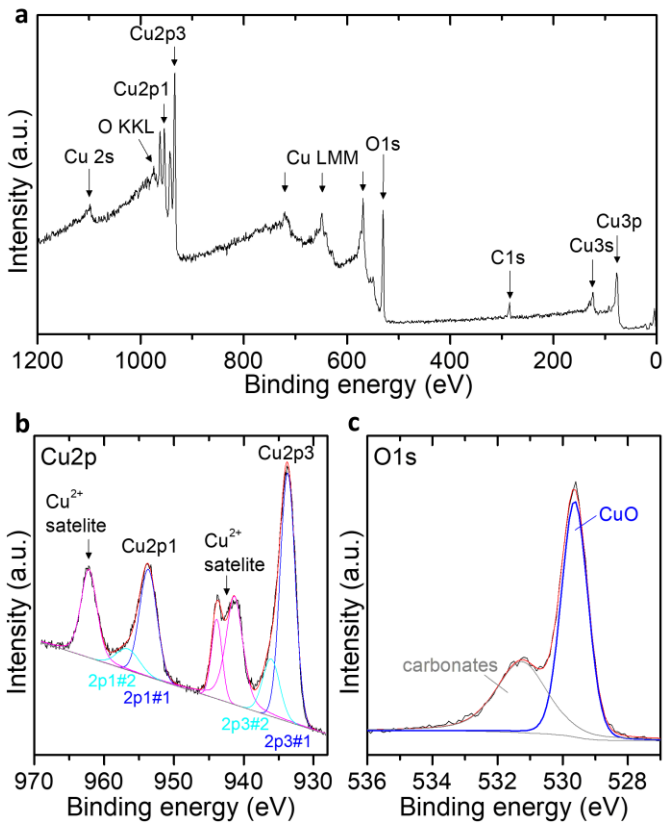

Figure S3. XPS spectra of a Si/CuO sample: Survey scan (a), and high-resolution scans of the Cu2p (b) and O1s (c) peaks.

Table S5. XPS peak fit data on CuO: The Cu2p and O1s peaks of Figure S3b and S3c are fitted by Gaussian-Lorentzian sum functions (*). The $Cu2p_{3/2}$/$Cu2p_{1/2}$ peak area ratios are constrained to 2/1 each (with Cu2p3 = $Cu2p_{3/2}$ and Cu2p1 = $Cu2p_{1/2}$). RSF values used for Cu:O peak ratio fitting are 2.93 (O1s), 8.66 (Cu2p1), 16.73(Cu2p3).

	Cu2p							O1s	
	2p1#1	**2p3#1**	**2p1#2**	**2p3#2**	**sat2p1**	**sat2p3#1**	**sat2p#2**	**carb.**	**CuO**
Pos. (eV)	953.68	933.71	956.6	936.07	962.18	943.34	943.87	531.26	529.63
FWHM (eV)	2.93	2.53	3.87	2.88	2.72	2.85	1.77	1.84	0.59
Area (a.u.)	13110	26221	3441	6881	11301	15387	5869	6374	9446
L:G* (%)	0	0	0	0	28	41	0	45	10

S3. Optical images of CuCDC, CuBDC and CP-CuBDC films

CuCDC (dry)

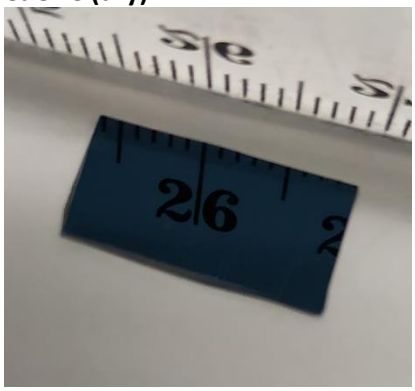

CuCDC (hum.)

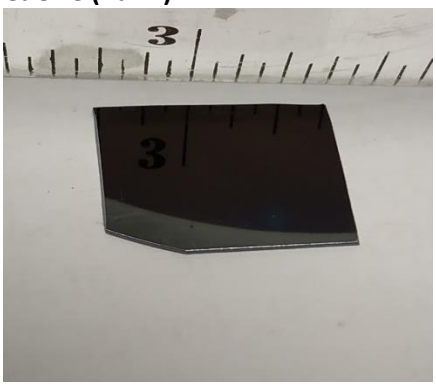

CuBDC

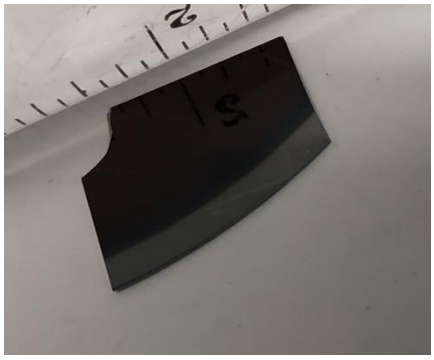

CP-CuBDC

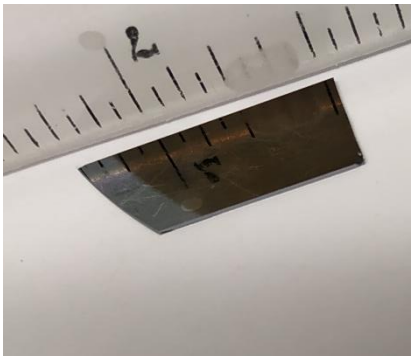

Figure S4. Images of CuCDC (top left, dry conditions), CuCDC (top right, humidified conditions), CuBDC (bottom left, dry conditions) and CP-CuBDC (bottom right, humidified conditions) mirror-like films with a colour ranging from deep blue to brown.

S4. CuCDC films from PVD CuO, PVD Cu and thermal CuO, on silicon and glass substrates

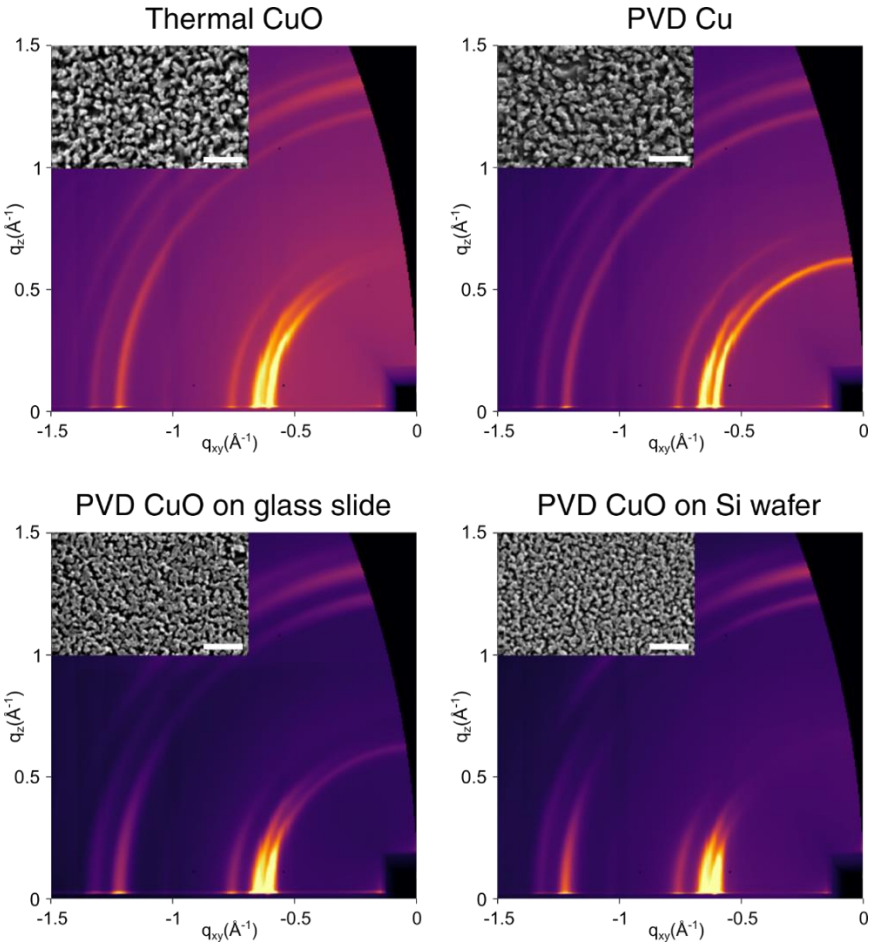

Figure S5. CuCDC films grown from thermal CuO on Si wafer substrate(top left), PVD Cu on Si wafer substrate (top right), PVD CuO on glass disk substrate (bottom left), and PVD CuO on Si wafer substrate (bottom right). Synchrotron GIXRD patterns (main) and SEM images (inset) with scale bar = 500 nm.

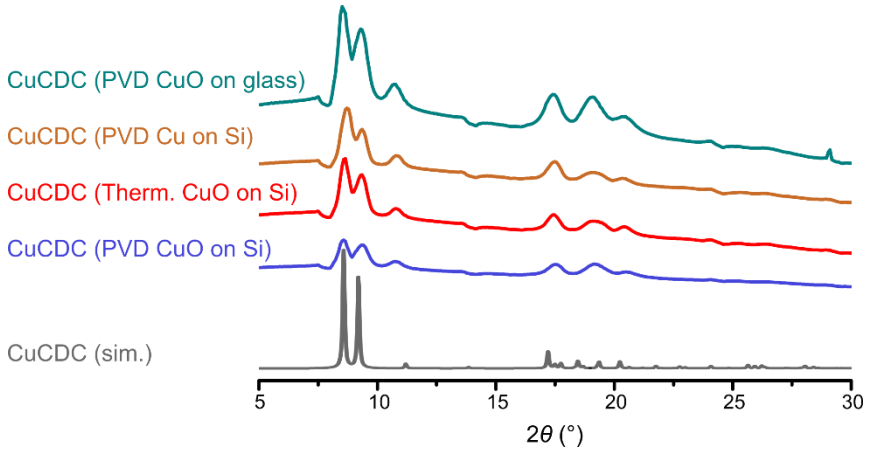

Figure S6. Intensity distribution as a function of 2θ extracted from GIXRD patterns displayed in Figure S5, and simulated PXRD pattern for CuCDC (grey, CSD = SIWGUB).

S5. CuBDC and CP-CuBDC films from PVD CuO, PVD Cu and thermal CuO, on silicon substrates

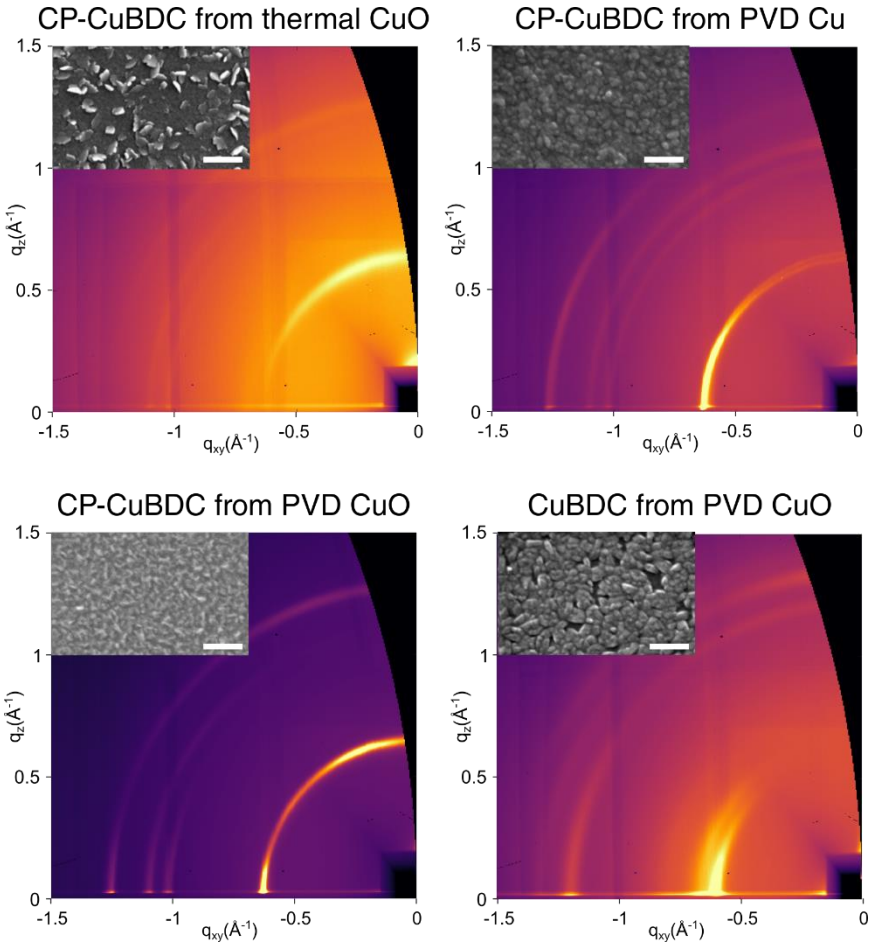

Figure S7. CP-CuBDC films grown under humidified conditions from thermal CuO on Si wafer substrate (top left), PVD Cu on Si wafer substrate (top right), PVD CuO on Si wafer substrate (bottom left), and CuBDC film grown under dry conditions from PVD CuO on Si wafer substrate (bottom right). Synchrotron GIXRD patterns (main) and SEM images (inset) with scale bar = 500 nm.

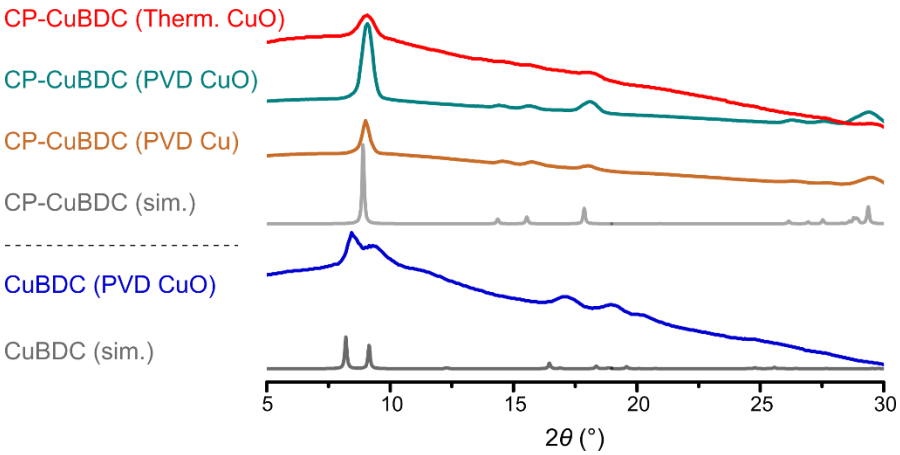

Figure S8. Intensity distribution as a function of 2θ extracted from GIXRD patterns displayed in Figure S7, and simulated PXRD pattern for CuBDC (dark grey, CSD = ZUBKEO) and CP-CuBDC (light grey, CSD = KAKSUL).

S6. AFM investigation of CuCDC, CuBDC and CP-CuBDC films

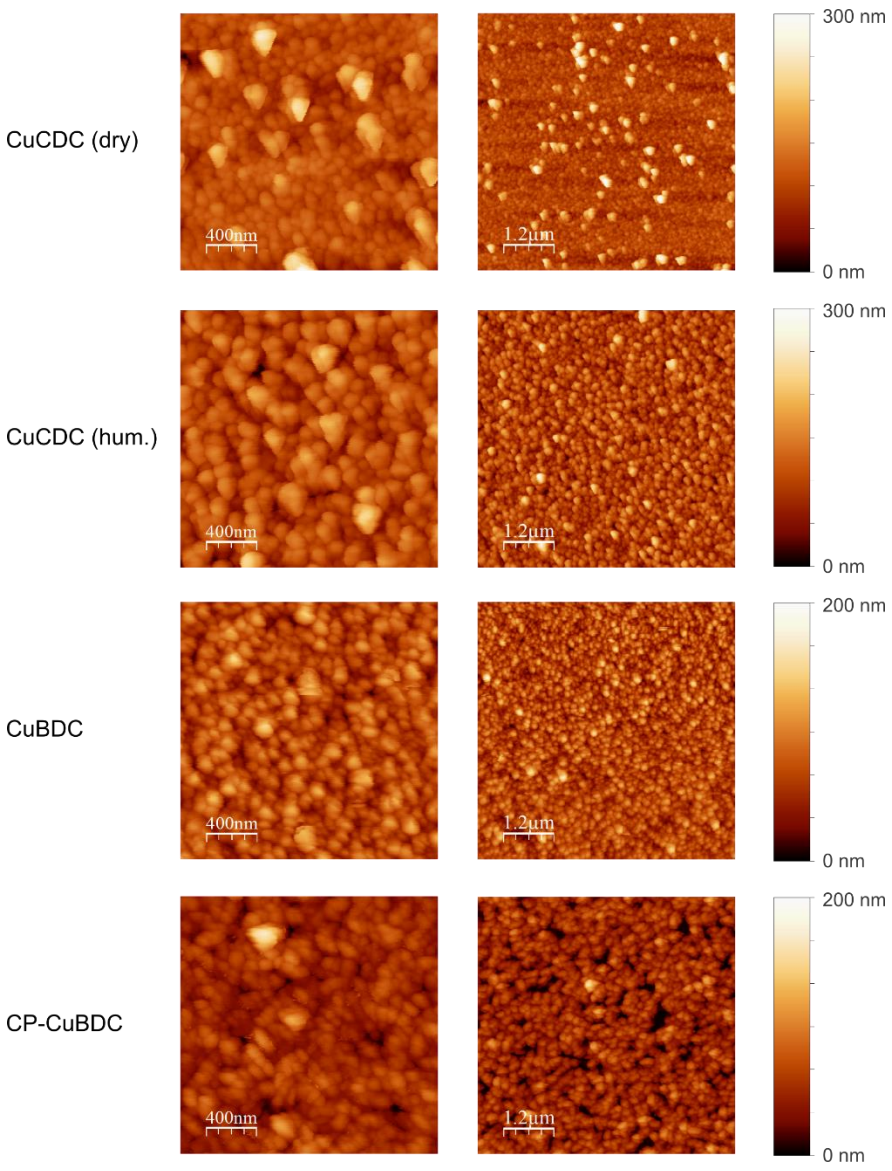

Figure S9. AFM images of CuCDC grown under dry conditions, CuCDC grown under humidified conditions, CuBDC grown under dry conditions and CP-CuBDC grown under humidified conditions. The films were analysed using a 2 x 2 µm² (left) and 6 x 6 µm² (right) probe area.

Table S6. Arithmetic (R_A) and root mean squared (R_{RMS}) roughness extracted from the AFM images. Reported values are for the 6 x 6 µm² probe area.

CuCDC (dry)		CuCDC (hum.)		CuBDC		CP-CuBDC	
R_A (nm)	R_{RMS} (nm)	R_A (nm)	R_{RMS} (nm)	R_A (nm)	R_{RMS} (nm)	R_A (nm)	R_{RMS} (nm)
21.3	30.6	24.0	30.2	16.7	21.4	12.5	17.0

S7. CuCDC, CuBDC and CP-CuBDC film thickness from ellipsometry data

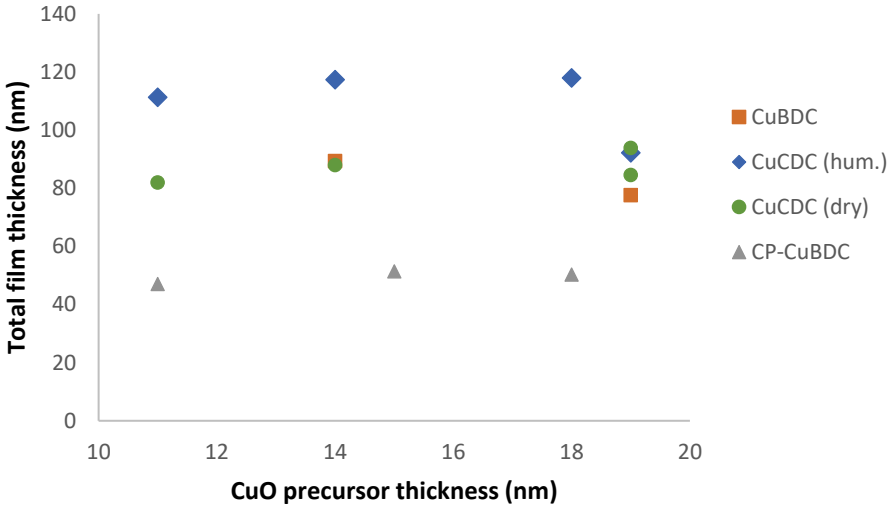

Figure S10. Total film thickness from ellipsometry data using a Cauchy model for CuCDC grown under dry (green circles) and humidified (blue diamonds) conditions, CuBDC (orange squares) and CP-CuBDC (grey triangles) as a function of PVD CuO precursor film thickness.

S8. Cross-sectional SEM images

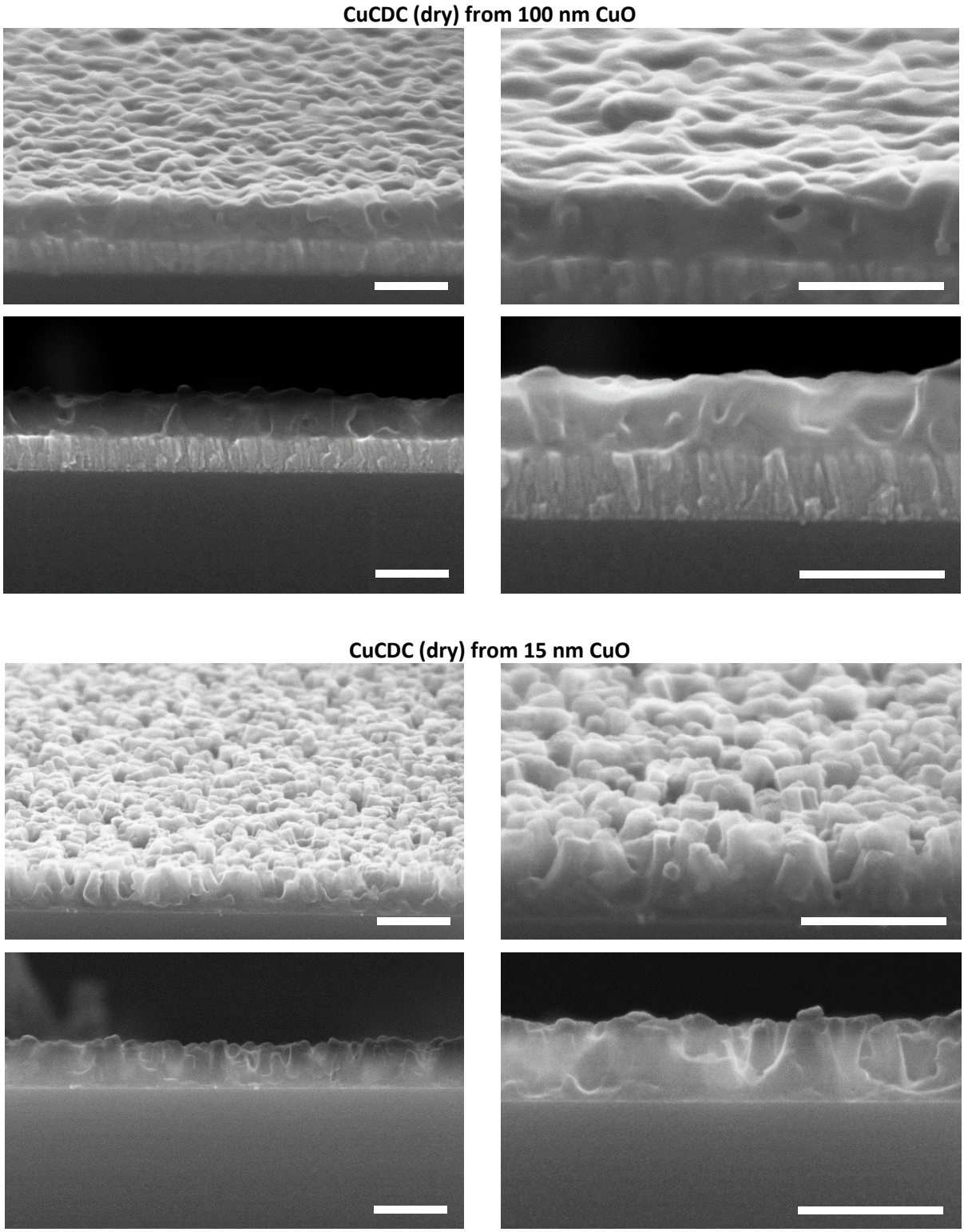

Figure S11. Tilted and cross-sectional view SEM images of CuCDC films grown from thick (~100 nm, top)) and thin (~15 nm, bottom) PVD CuO. Scale bar = 200 µm.

S9. H_2BDC and H_2CDC linker thermogravimetric analysis

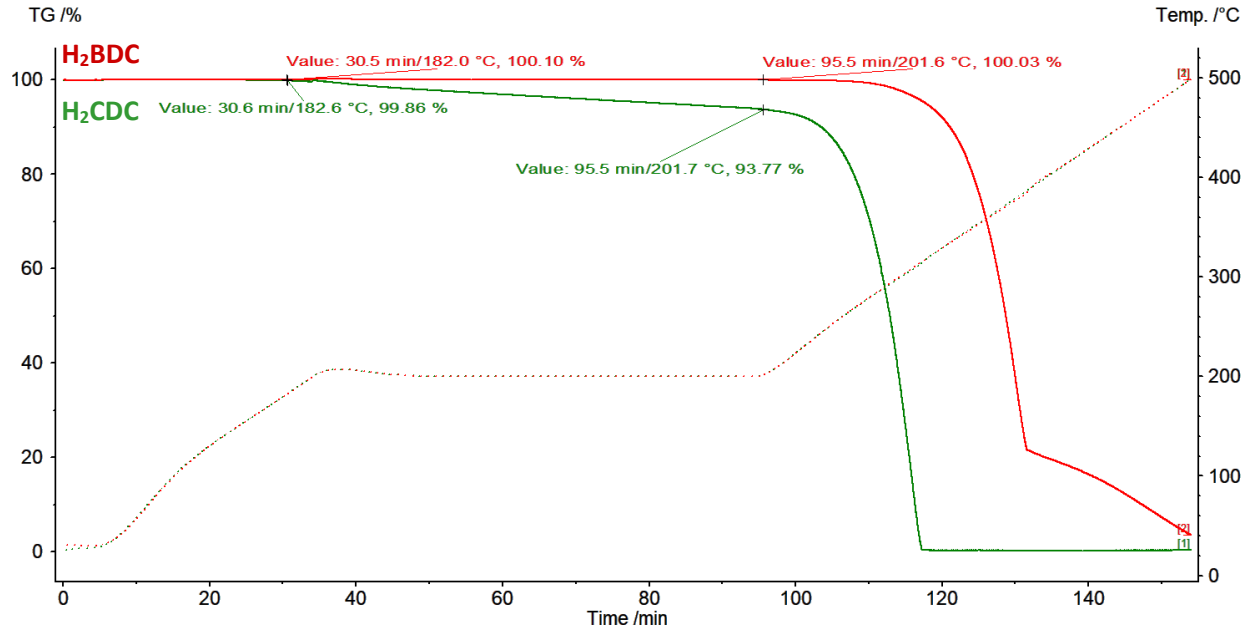

Figure S12. Thermogravimetric curves (full lines) and temperature profile (dotted lines) of H_2BDC (red) and H_2CDC (green) measured under nitrogen atmosphere. The larger weight loss at any temperature of H_2CDC in comparison to H_2BDC evidences the higher volatility of H_2CDC in comparison to H_2BDC.

S10. ATR-FTIR analysis

FTIR spectra and band assignment

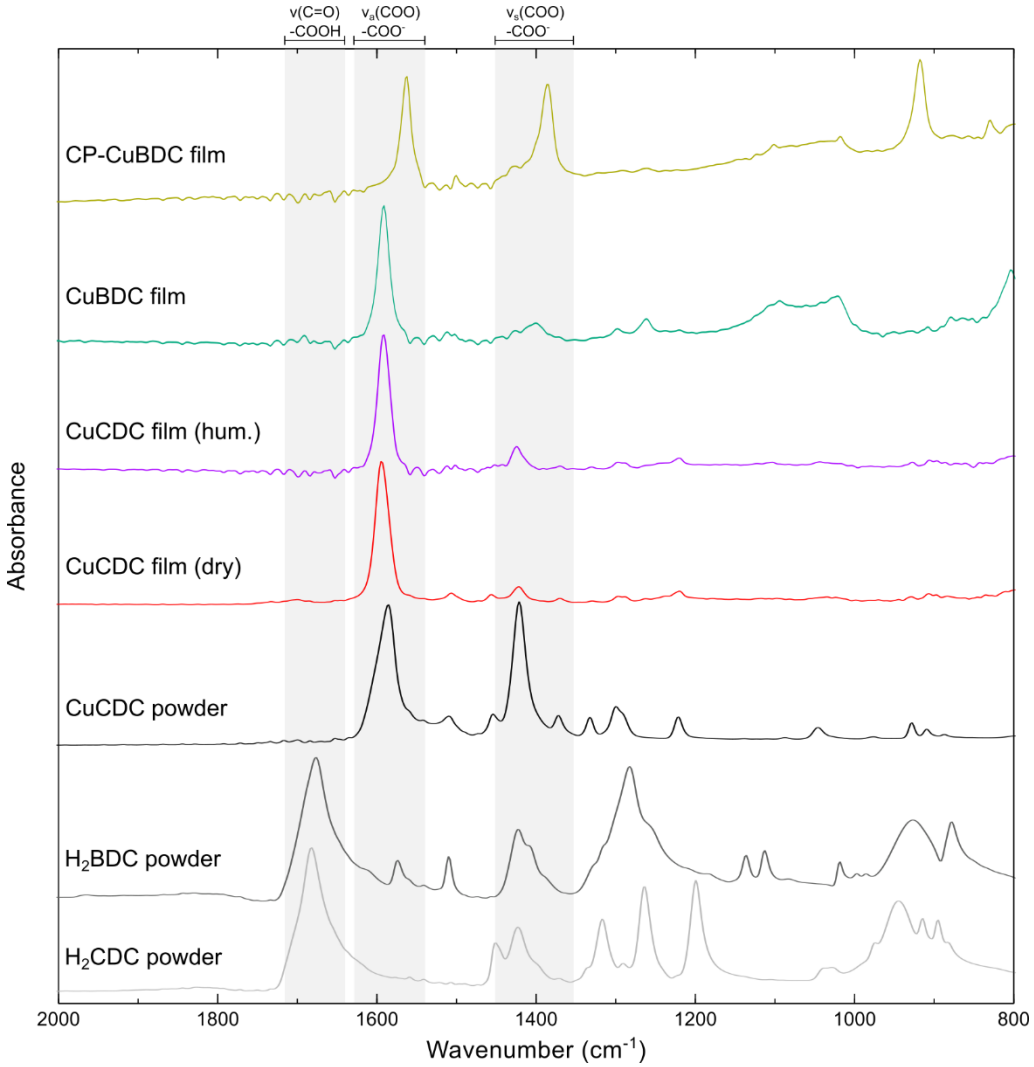

Figure S13. ATR-FTIR spectra for CuBDC, CuCDC and CP-CuBDC thin films, and solvothermally synthesized CuCDC, H_2BDC and H_2CDC powders. The carboxylic acid and carboxylate band location are highlighted as grey boxes.

Table S7. FTIR band frequencies and assignment, and ratio of carboxylate bands absorbance as metric for CuCDC and CuBDC film orientation.

	ν(C=O) -COOH (cm^{-1})	**ν_{asym}(COO) -COO$^-$ (cm^{-1})**	**ν_{sym}(COO) -COO$^-$ (cm^{-1})**	**Abs(ν_{asym})/Abs(ν_{sym})**
CP-CuBDC film	-	1563	1385	1.1
CuBDC film	-	1591	1400	6.7
CuCDC film (hum.)	-	1592	1424	6.2
CuCDC film (dry)	-	1594	1422	8.7
CuCDC powder	-	1586	1421	1.0
H_2BDC	1676	-	-	-
H_2CDC	1682	-	-	-

Dihedral angle between carboxylate groups planes and (100) crystal plane

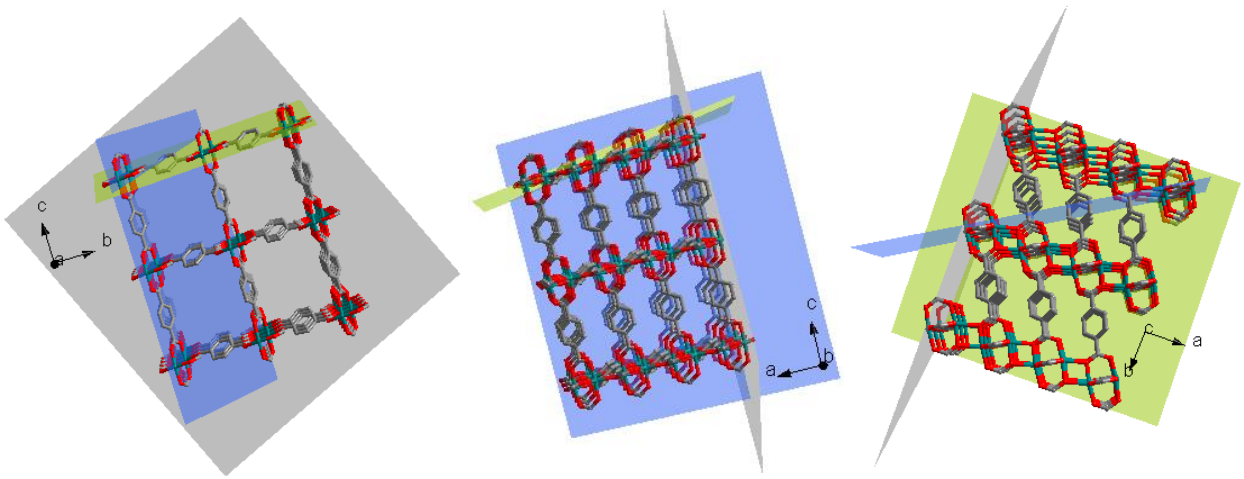

Figure S14. The carboxylate groups in both CuCDC (not depicted) and CuBDC (depicted) define two family of crystal planes, with one such plane per family depicted in blue and green, respectively. The (100) crystal plane is depicted in green.

Table S8. Calculated dihedral angle between carboxylate planes and (100) crystal plane for CuCDC and CuBDC.

	Dihedral angle	**Carboxylate fraction**
CuCDC	85°	0.5
	55°	0.5
weighted average	**70°**	
CuBDC	82°	0.5
	58°	0.5
weighted average	**70°**	

S11. CuBDC oriented films: liquid-phase epitaxy vs CVD

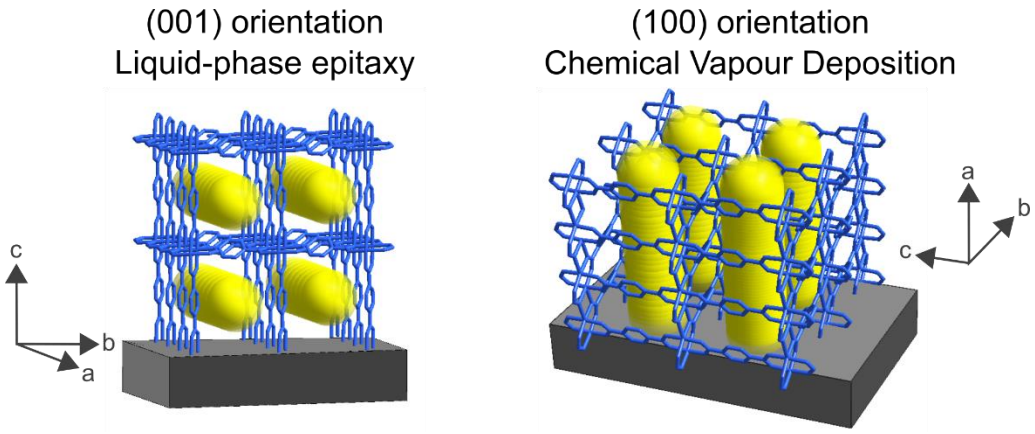

Figure S15. Schematic representation of oriented CuBDC thin films: (001) orientation with pores running parallel to the substrate as obtained by liquid-phase epitaxy[5] (left) and (100) orientation with pores running perpendicular to the substrate as obtained by chemical vapour deposition (right, this work).

S12. References

1 B. Schrode, S. Pachmajer, M. Dohr, C. Röthel, J. Domke, T. Fritz, R. Resel and O. Werzer, *J. Appl. Crystallogr.*, 2019, **52**, 683–689.

2 I. Horcas, R. Fernández, J. M. Gómez-Rodríguez, J. Colchero, J. Gómez-Herrero and A. M. Baro, *Rev. Sci. Instrum.*, 2007, **78**, 013705.

3 R. P. Vasquez, *Surf. Sci. Spectra*, 1998, **5**, 262–266.

4 R. P. Vasquez, *Surf. Sci. Spectra*, 1998, **5**, 257–261.

5 J. Liu, B. Lukose, O. Shekhah, H. K. Arslan, P. Weidler, H. Gliemann, S. Bräse, S. Grosjean, A. Godt, X. Feng, K. Müllen, I.-B. Magdau, T. Heine and C. Wöll, *Sci. Rep.*, 2012, **2**, 921.